ASSESSING THERMAL BARRIER COATINGS BY INVERSION OF EDDY-CURRENT IMPEDANCE DATA[1]

Harold A. Sabbagh, Elias H. Sabbagh, R. Kim Murphy
Victor Technologies, LLC, PO Box 7706, Bloomington, IN 47407-7706 USA
John Nyenhuis, Purdue University, West Lafayette, IN 47907-1285 USA

The nondestructive evaluation (NDE) of high temperature coatings is one of the important factors in achieving a high level of structural integrity in advanced gas turbines. In this paper, we demonstrate that sophisticated eddy current techniques can be utilized to measure the thickness and remaining life of high temperature coatings. Some research has been conducted to apply such techniques to the preservice case, for which the coating has one nicely defined layer and nothing of consequence has diffused into the base metal that would create additional layers of anomalous material. We discuss the much more difficult inservice case, in which the time temperature exposure of the combustion turbine blade has created a four layered system, in addition to the base metal. The particular coatings that we discuss are made up of NiCoCrAlY with a top aluminide coating, GT33+, and without the top aluminide coating, PWA286.

[1]Presented at the 16th World Conference on Nondestructive Testing, Montreal, Friday, 03SEP04.

INTRODUCTION

Advanced turbines, such as the GE Frame 7FA/9FA, are used in applications ranging from aerospace to land-based power generators. These turbines are fired at higher temperatures (1850°F–1950°F), and utilize optimum cooling of hot section components. Because of the higher operating temperature, the performance and durability of the first stage blades has become one of the prime life-limiting factors. Individual blades are nickel-based GTD111 alloys, that are protected by sacrificial metallic coatings to extend service life. The first-stage blades are especially important, and it is desirable to develop an *in-situ* NDE system to monitor, evaluate, and predict remaining coating life. The coatings used on the turbine blades include CoCrAlY and NiCoCrAlY, with a top aluminide coating (GT29+, GT33+, respectively), and a NiCoCrAlY coating, called PWA 286 [1].

Victor Technologies has been performing research into the nondestructive characterization of in-service high-temperature metallic (such as MCrAlY) thermal barrier coatings (TBC) applied by vacuum plasma spray on Ni-based superalloy turbine blades. In this report we describe our efforts in applying **VIC-3D©** to the problem of characterizing the GT33+ duplex coating.

THE GT33+ DUPLEX COATING

The GT33+ duplex coating has two layers of beta aluminide, an especially rich one, called $\beta+$, having a conductivity of about 1.2×10^6 S/m, and a 'normal' one, called β, with a conductivity of about 8.4×10^5 S/m, as in the PWA286 coating. In addition, there is the usual aluminum oxide layer (Al_2O_3) that is the actual thermal barrier above $\beta+$, and an inter-diffusion zone (IZ) with a nominal conductivity of 3.2×10^5 S/m between β and the GTD111 substrate. We have not studied the IZ in this report, because it is small (as in the case of the PWA286) and less important in determining the remaining life of the coating. The GTD111 substrate is identical to the one studied earlier, and has a nominal conductivity of 7.8×10^5S/m.

Figure 1 shows the 'electrical profile' of the GT33+ coating. The figure suggests that the $\beta+$ and β layers may have different thicknesses, but metallurgical measurements on various samples suggest that the two layers have comparable thicknesses, which we take to be 100μm. Trying to assess the thickness of the IZ layer in the face of the large combined thickness of the aluminide layers seemed unwise, and that is one reason for ignoring the presence of IZ in our studies.

Thus, our inversion problem becomes one of determining the thickness of the Al_2O_3 layer (Z2), which has a known conductivity of 0 S/m, and determining the conductivity of the $\beta+$ and β layers, each of which is 100μm thick. We should mention that it is a bit disconcerting to identify a layer by a fixed chemical/metallurgical name, such as $\beta+$ or β when its electrical conductivity may change. It seems to us that the electrical and chemical/metallurgical properties should be tied together, so that if the electrical conductivity changes, then so should the chemical name of the layer. We will adapt the convention, however, that the two layers retain their same names, even if their conductivities should change, and even if the conductivity of the β layer should become higher than the $\beta+$ layer!

All coatings form a thin protective adherent layer of Al_2O_3 [2],[3]. As the protective oxide spalls off during service, aluminum in the coating diffuses out to re-form the protective oxide layer, and also diffuses into the substrate and causes the interdiffusion zone to increase in thickness.

Figure 2 illustrates a micrograph of a GT33+ coating. At the top is a NiAl overlay coating, followed by the NiCoCrAlY bond coat and the inter-diffusion layer. The GTD111 substrate is the light-colored region at the bottom.

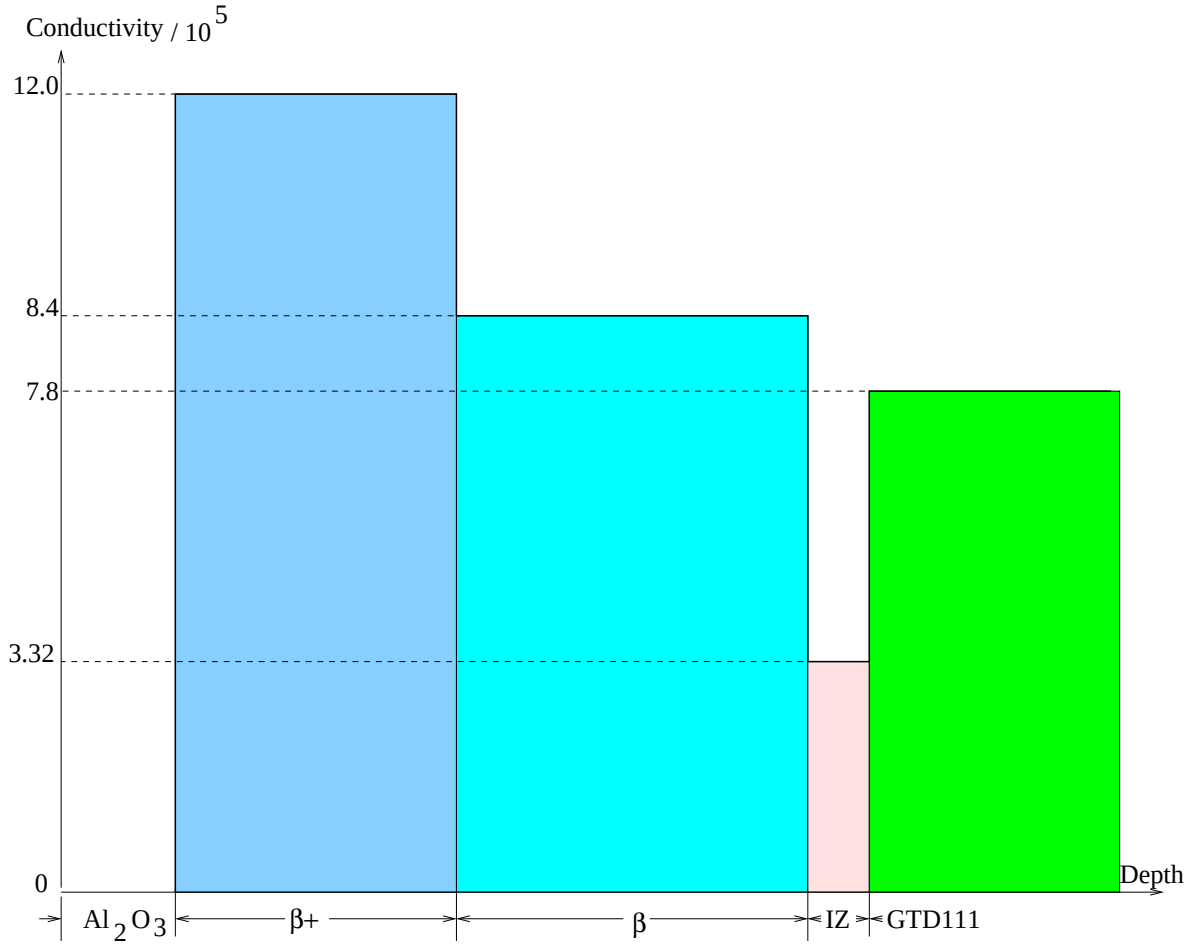

Figure 1: The electrical profile of the GT33+ coating. In the reconstructions we assume that the thickness of the $\beta+$ and β layers are each equal to 100μm. The GTD111 substrate, of course, extends to infinity.

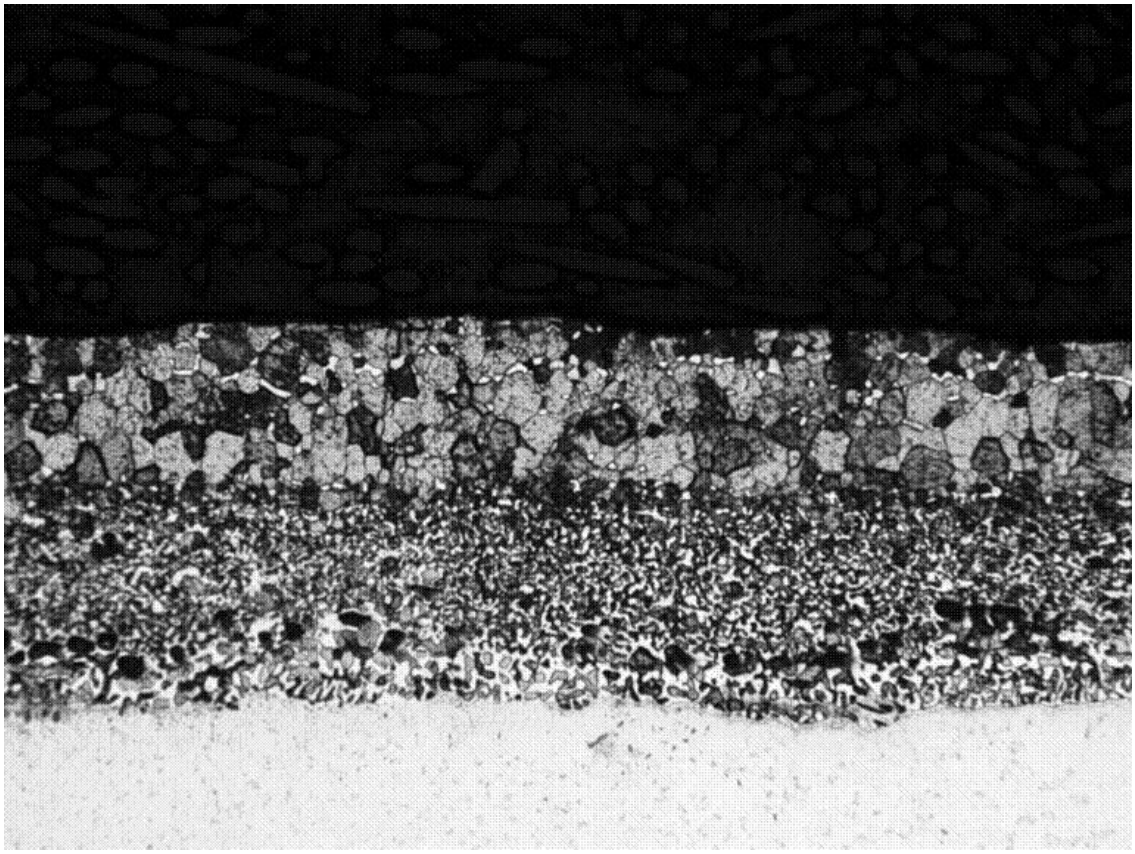

Figure 2: Micrograph of a sample of GT33+ duplex coating, comprising a top NiAl overlay coating, followed by the NiCoCrAlY bond coat and the inter-diffusion layer. The GTD111 substrate is the light-colored region at the bottom .

The primary objective is to estimate the equivalent conductivity of the overlay and bond coatings, assuming a fixed thickness of each coating of roughly 100μ. This information is essential to maintaining the integrity of blades, because it allows the timely repair or refurbishment of coatings to extend the service-life of operating blades. Further, it is desirable to obtain the β-phase depleted zone 2 (Al_2O_3) thickness, since this information indicates the level of blade exposure to service temperature. The overall remaining coating thickness indicates the reduction of the coating thickness caused by the oxidation-induced degradation of the top beta-phase depleted layer [1].

We have performed a number of model calculations of the TBC problem, using our proprietary eddy-current NDE code, **VIC-3D©** and have determined important system features, such as operating frequency, coil characteristics, electronic test equipment considerations, and means of accelerating the computations. As a result, we have concluded that the optimum frequency range for performing the inversions required of the TBC problem is 1 MHz to 50 MHz. Successful inversions in this range will allow us to achieve the desired resolution for these extremely thin coatings.

Because there are no commercially available eddy-current instruments that operate in this frequency range, we used the Hewlett-Packard HP 3577A Network Analyzer, that is designed to operate over the frequency range of 5Hz to 200MHz. This instrument measures the reflection coefficient of a one-port network (namely, the loaded coil), from which the impedance data, that are the input to the inversion algorithm, are determined.

There are several steps to be carried out during the testing. First will be to characterize the probe in free-space, then to collect the impedance data, and finally to invert these data using our '8-layer algorithm.'

DATA COLLECTION

Figure 3 illustrates an actual turbine blade. The suction side faces the viewer, with the leading edge to the right. The chord length is measured along the suction side from the leading edge to the trailing edge.

The samples used in the PWA286 project were flat coupons, so the fact that the coil is embedded in a large acrylic box was unimportant. The present samples, however, were sections of actual turbine blades, which means that their 'active' areas of interest are curved, having a suction and pressure side. We were able to inspect the sample at only one point on the suction side, because that is the only point of tangency of the blade over the coil. We positioned the blade so that the point of tangency lay on the midplane of the suction side, and that is where the measurements were taken. See Figure 4.

The test positions relative to the chord length from the leading edge on the suction side are shown in Table 1.

Sample	A	B	E
Test spot from leading edge (in)	4.5	3.5	3.0
Total chord length from leading edge (in)	7.5	6.5	5.75
Percent of test spot to chord length	60	54	52

Table 1: Relative test positions on the samples.

Using the HP network analyzer and the Zetec coil, we measured the reflection coefficient, S_{11}, of the loaded coil, from one to fifty megahertz, in one-megahertz steps, for each of the test samples.

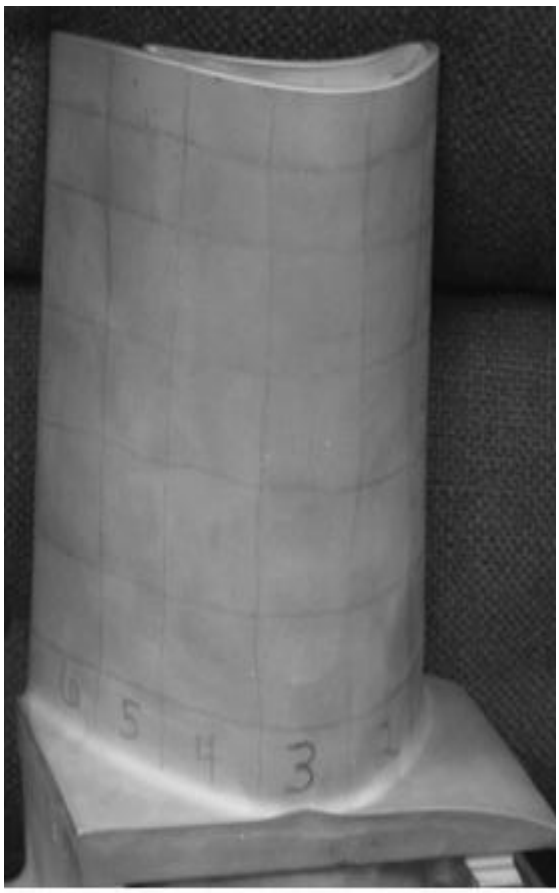

Figure 3: Showing a section of an actual turbine blade. The suction side faces the viewer, with the leading edge to the right. The chord length is measured along the suction side from the leading edge to the trailing edge.

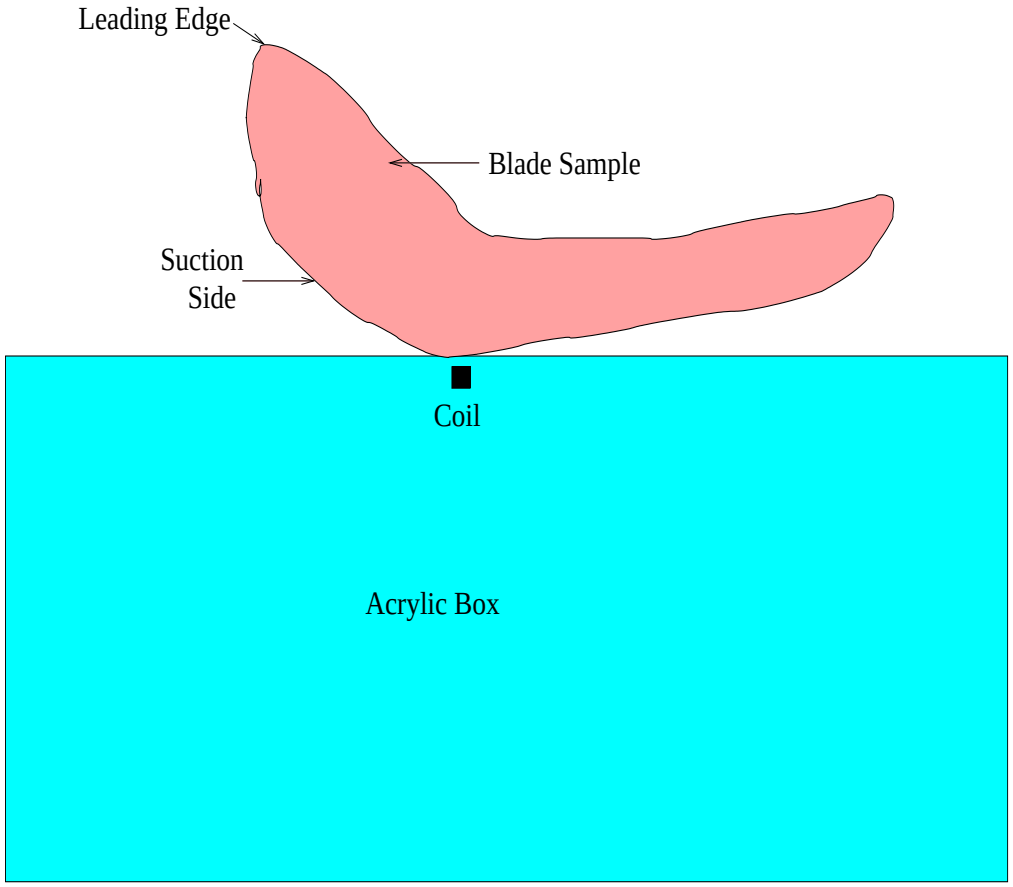

Figure 4: Showing the position of the blade sample on the acrylic box over the coil. One point on the suction side, only, was used.

S_{11} is recorded as a magnitude and phase (in degrees). Z_W, the change in normalized impedance due to the workpiece, is then computed from the scattering coefficients. (By 'normalized,' we means that the true data at each frequency have been divided by the reactance of the probe coil in freespace, at that frequency.) The real and imaginary parts of the normalized impedances for the four test samples are shown in Figures 5-8.

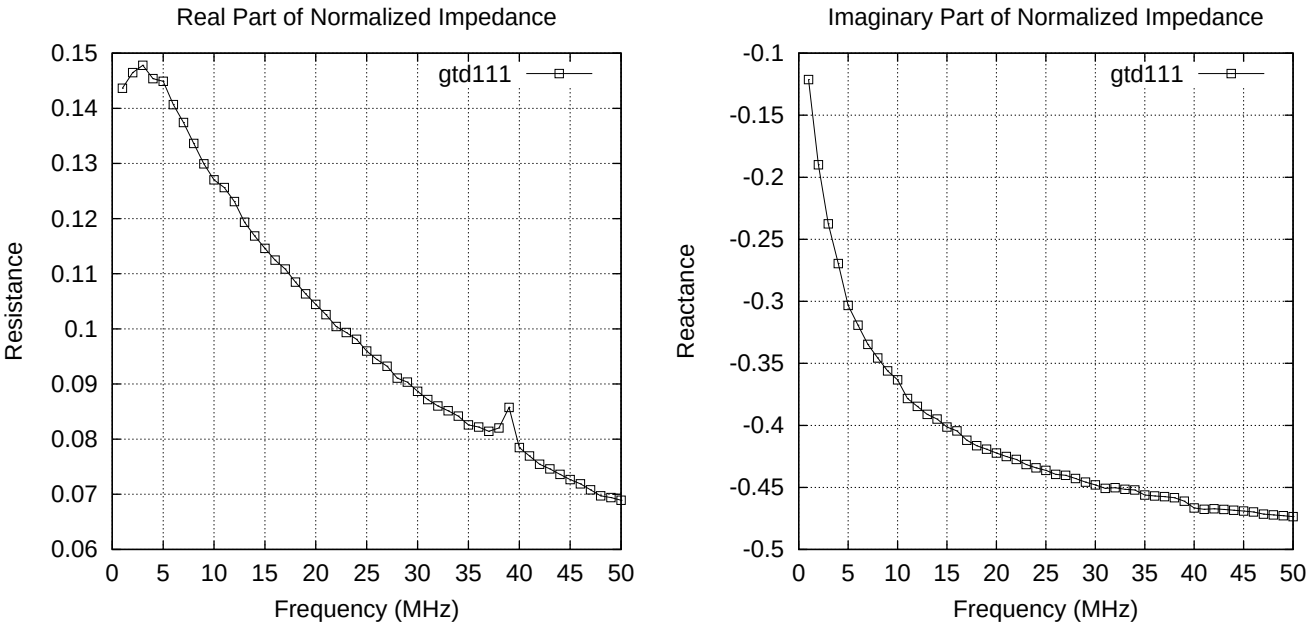

Figure 5: Real (left) and imaginary (right) parts of the normalized impedances for the GTD111 substrate.

Z_W is recorded as a change in resistance (real part), and a change in reactance (imaginary part). The change in reactance is always negative (due to Lenz' law), whereas the change in resistance is positive.

The impedance data that are shown in Figures 5-8 are much noisier, or at least, less smooth than the data that we took for the PWA286 project, even though we used the same algorithms and frequency range to produce the data. Indeed, we were unable to even reproduce the impedance of the coil in free-sapce that we had in the earlier project.

There are two likely reasons for this, the first being that the network analyzer that we used for the GT33+ measurements was not the same as for the PWA286, and, in fact, may have some drift in it. (We had taken great pains to repeatedly calibrate the instrument over the entire frequency range.) The second possibility, which we think is more likely, is that the acrylic box that houses the coil may have aged in some manner, so that it actually presents a load on the system at the frequencies of interest. The fact that the data are noisy has some effect on the interpretation of the reconstructions, but not to the extent that we are unable to draw reasonable conclusions, as the next section shows.

RECONSTRUCTIONS USING MEASURED IMPEDANCE DATA

In inverting the GT33+ problem for Samples A, B and E, we didn't use the N-layer algorithm, which will be described shortly, because it was easier to simply use **VIC-3D©** to generate impedance

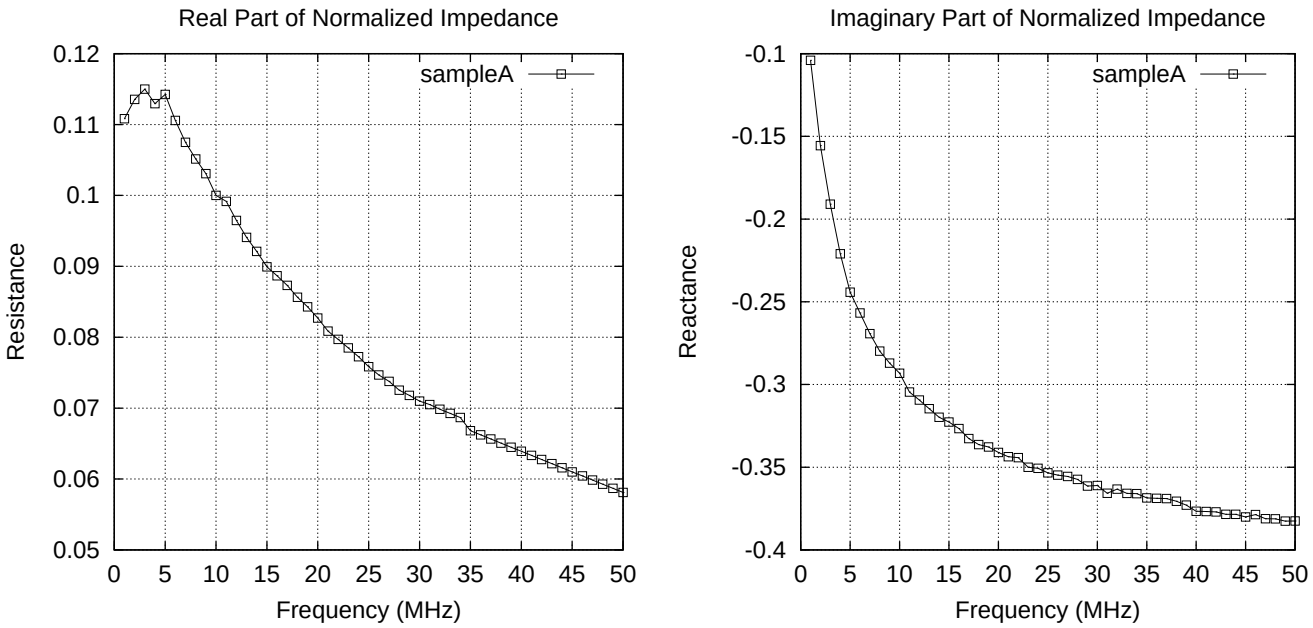

Figure 6: Real (left) and imaginary (right) parts of the normalized impedances for Sample A.

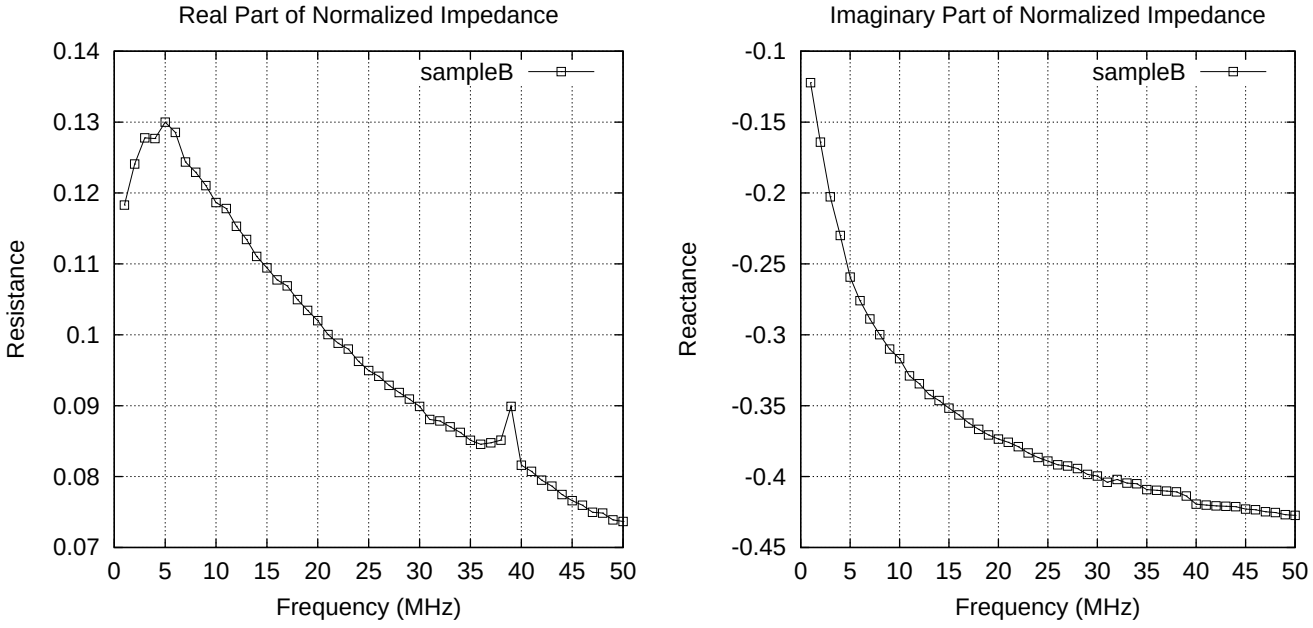

Figure 7: Real (left) and imaginary (right) parts of the normalized impedances for Sample B.

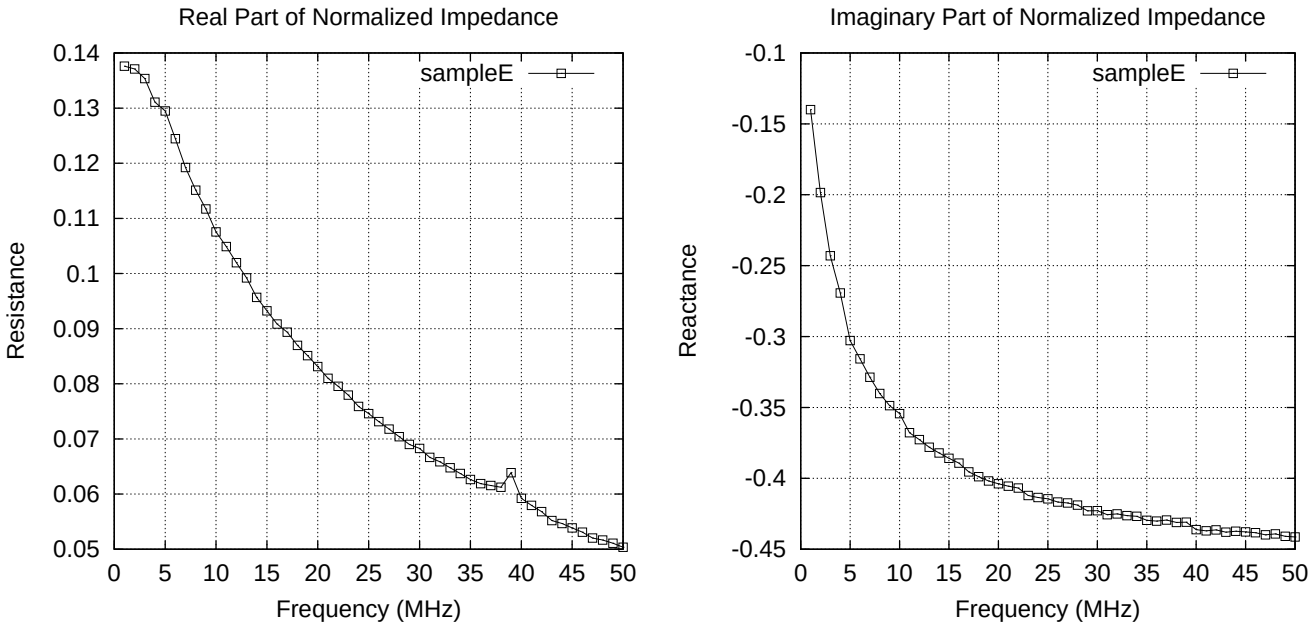

Figure 8: Real (left) and imaginary (right) parts of the normalized impedances for Sample E.

data. These data were then compared to the measured data of Figures 6-8. In a sense, we solved the inversion problem 'by hand.' The reason for this is that there are only three parameters to fit into the GT33+ model, namely Z_2, the thickness of the Al_2O_3 layer, and the conductivity of $\beta+$ and β. Further, we wanted to see exactly how the computed/measured data fit the simple model of the GT33+ coating–namely, one in which we assumed that the $\beta+$ and β thicknesses were fixed at 100 microns, and we ignored IZ. We also wanted to see how the high-frequency data could be used to determine the thickness of the Al_2O_3 layer and the $\beta+$ conductivity, and the low-frequency data help determine the conductivity of the β layer. Therefore, we simply ran a number of test models using **VIC-3D©** and then plotted the best fits with the measured data over the entire frequency range. This not only gives us the answer to the coating-thickness question, but also informs us as to the quality of the fit over the wide frequency range that we used. The results are shown in Figures 9-12.

In Figure 9, we present the results for the GTD111 substrate. The legend corresponds to three trial values of the coil liftoff in mils. The conductivity of the substrate is assumed to be 7.8×10^5 S/m, as for the PWA286 coating. The purpose of this study is to determine the effective coil liftoff, which is necessary to know in order to determine the thickness of the Al_2O_3 coating for Samples A, B and E. Further, it validates our assumption that the conductivity of the substrate is in fact 7.8×10^5 S/m. We see that the imaginary data fit the model over the entire frequency range better than the real. This observation holds almost uniformly for the other samples.

In Figure 10 we present results for Sample A. The three trial parameters are the thickness (in microns) of Z2 (Al_2O_3) and the conductivities of $\beta+$ and β. Again, we see that the reactance data lie more systematically between the two trial results than the resistance data.

Sample B results are shown in Figure 11. The trial parameters are the same as in Figure 10, but, of course their values are different. Clearly, the resistance behaves much more erratically than the reactance, and each gives conflicting results. The high-frequency resistance tends to be closer to the combination $\beta+ = 7 \times 10^5$, $\beta = 5 \times 10^5$, whereas the high-frequency reactance favors the

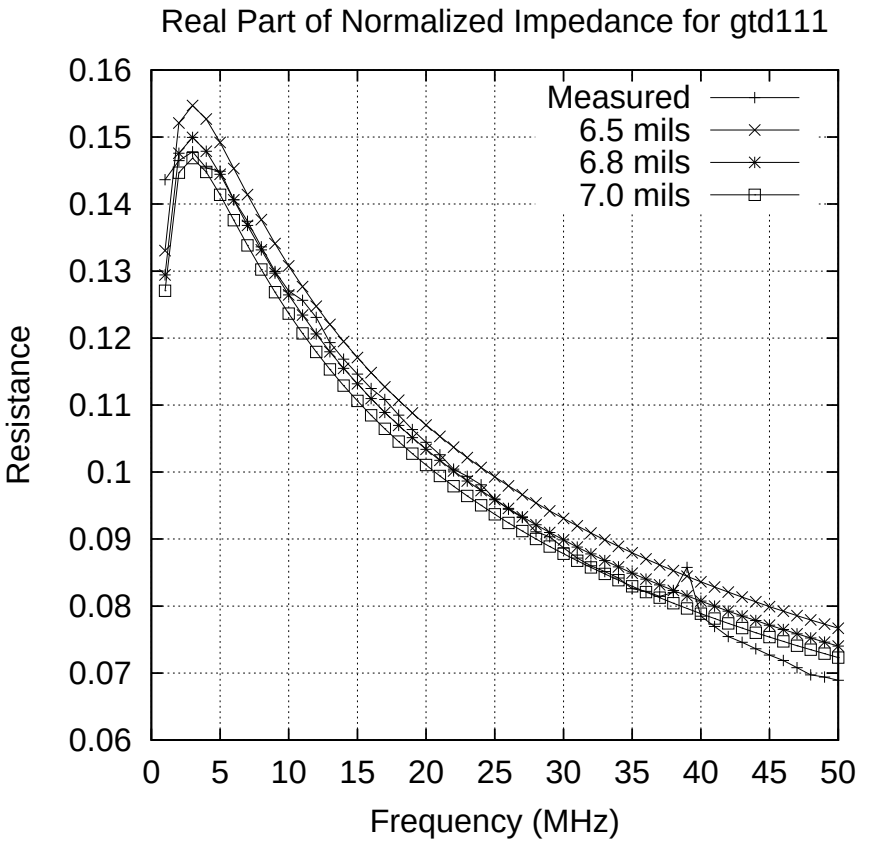

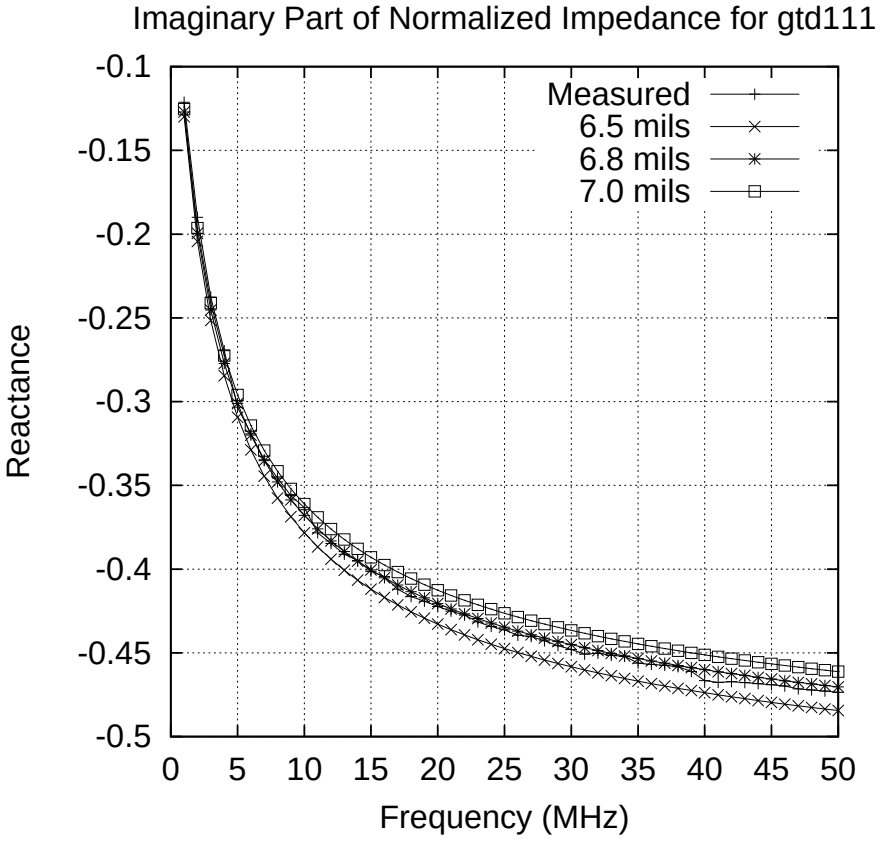

Figure 9: Results for GTD111.

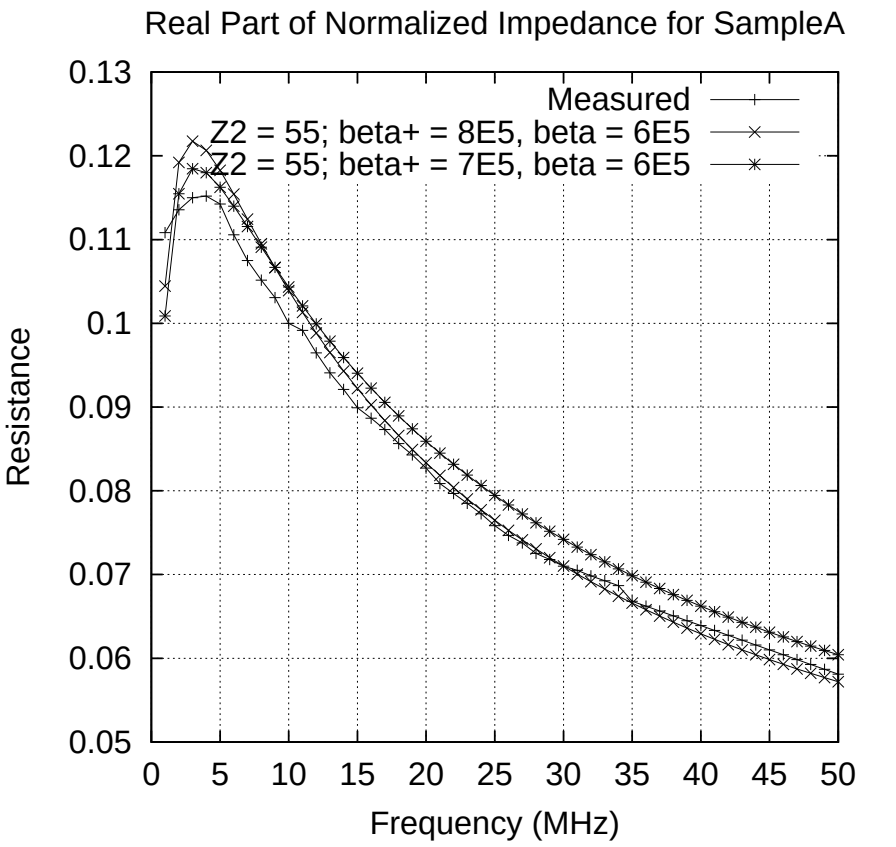

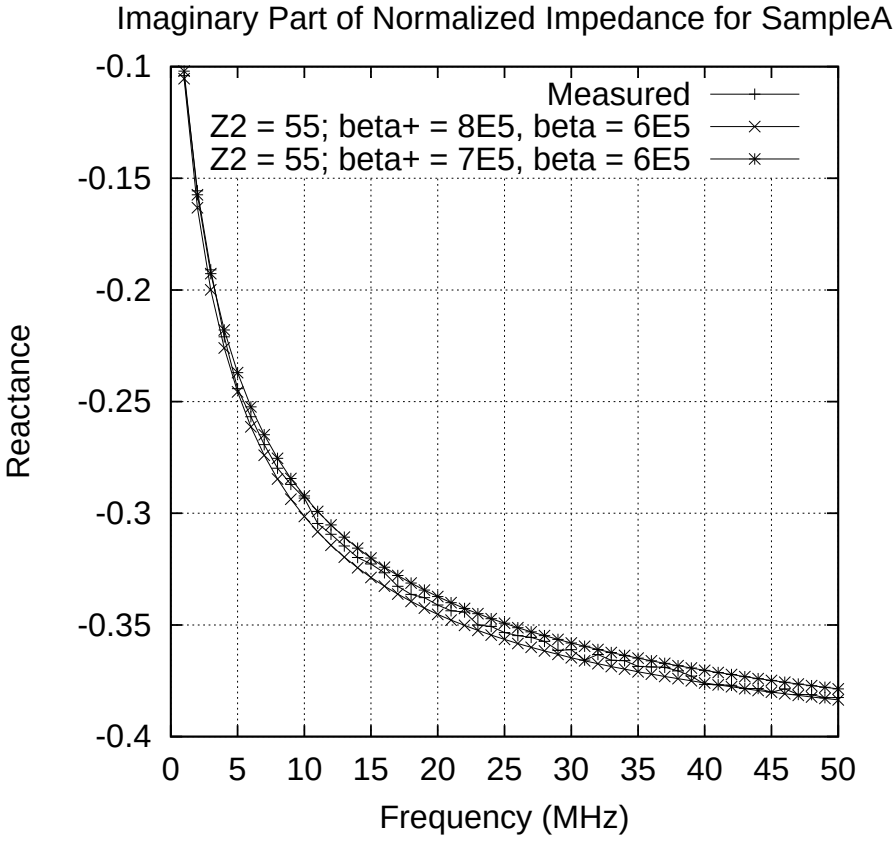

Figure 10: Results for Sample A.

combination $\beta+ = \beta = 5 \times 10^5$. The Sample E results are more consistent, as shown in Figure 11. The trial parameters are identical to the previous two (except, again, the values are different).

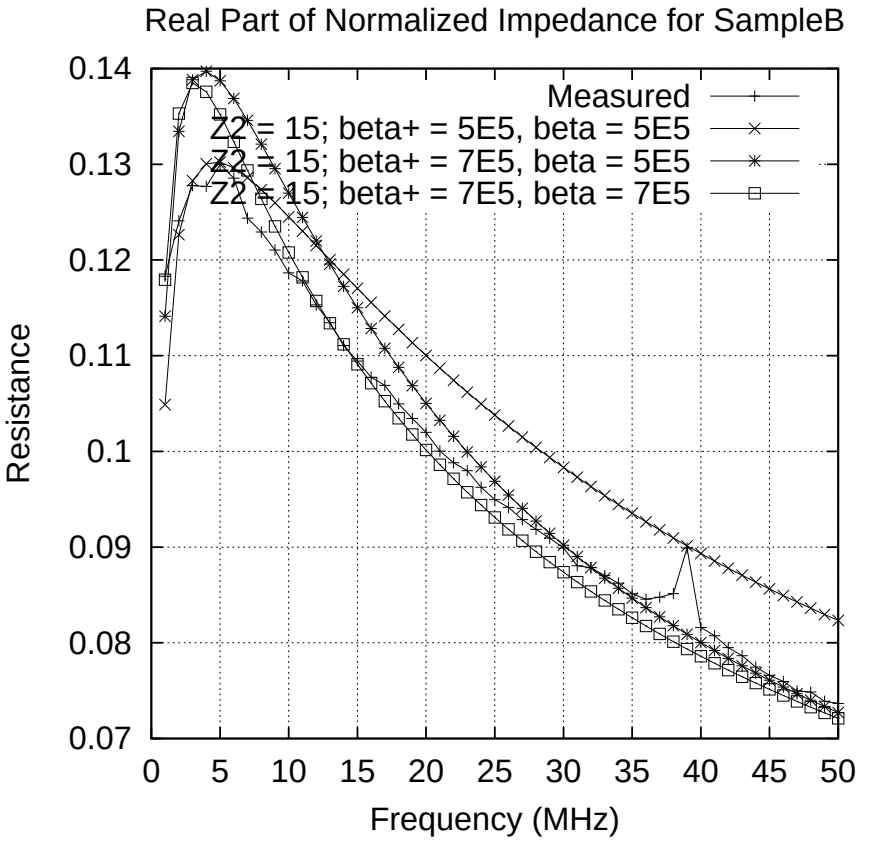

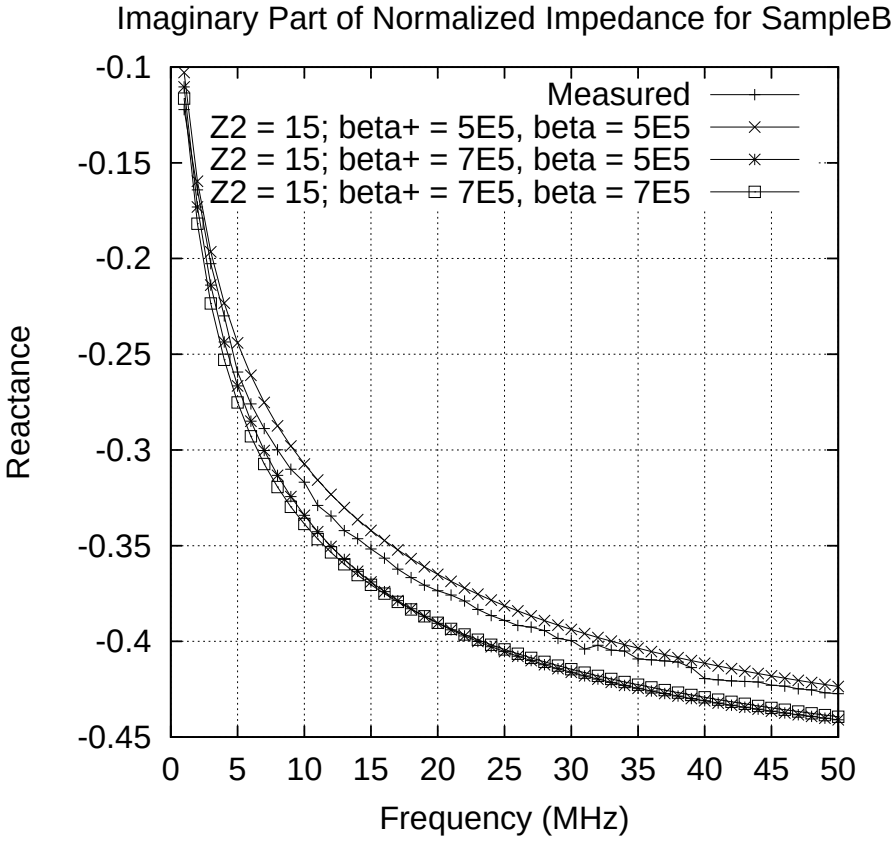

Figure 11: Results for Sample B.

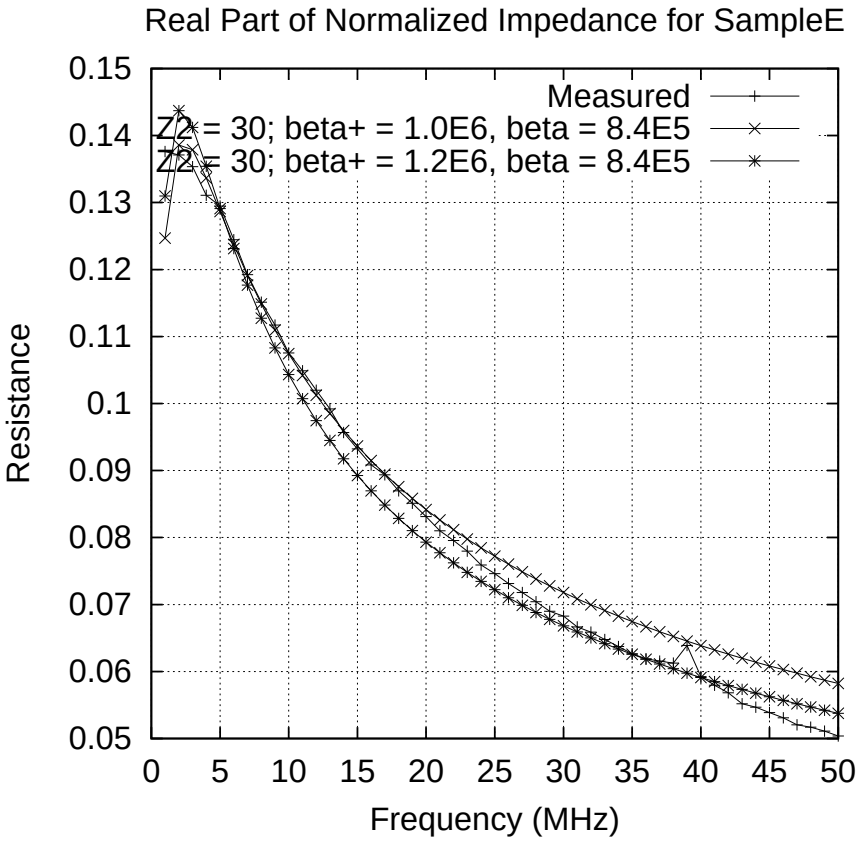

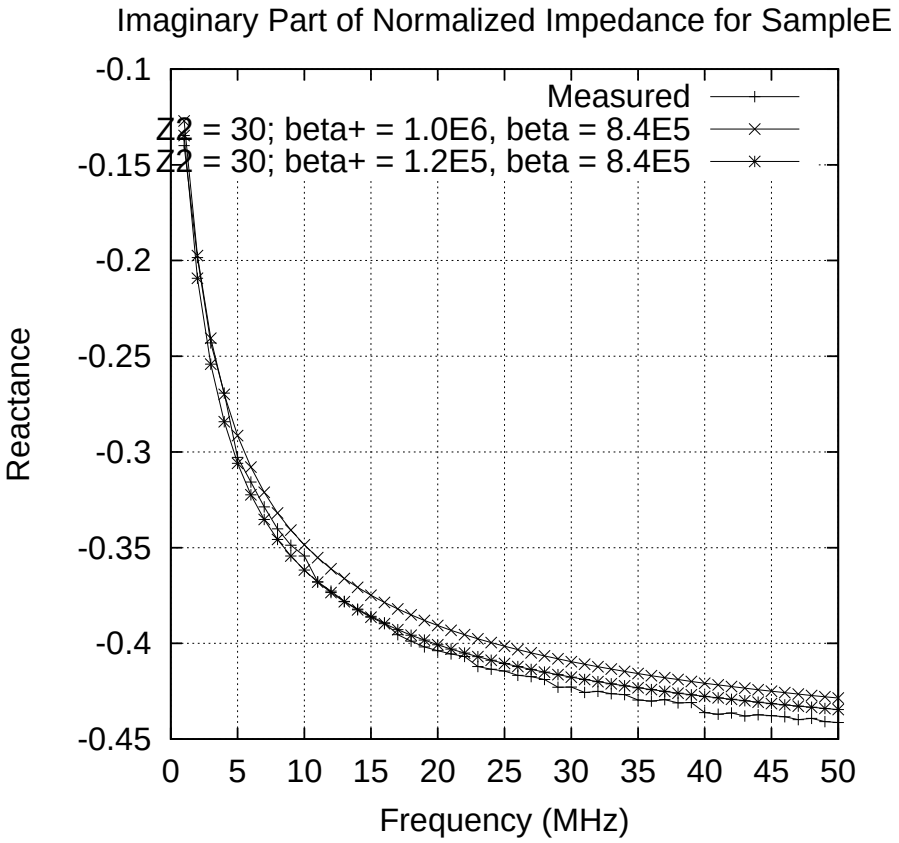

Figure 12: Resulst for Sample E.

INVERSION VIA THE N-LAYER ALGORITHM

The reconstruction of the GT33+ problem was accomplished without any sophisticated inversion algorithms because there were only three variables of interest. Generally, however, inverse problems contain many variables, and cannot be solved by hand. We have developed a very robust algorithm, called the N-layer algorithm, that allows us to efficiently compute layer thicknesses for thermal-barrier coatings (as well as myriad other problems). We have applied this algorithm to thermal-barrier coatings using eight to twelve layers; Figure 13 illustrates the configuration for eight layers.

Inverting the impedance data via the 8-layer algorithm means assigning a value to L_0, the thickness of the top layer of Figure 13, and assigning conductivities to the remaining seven layers, each of which has the same thickness, L, that defines the resolution of the reconstruction. This is

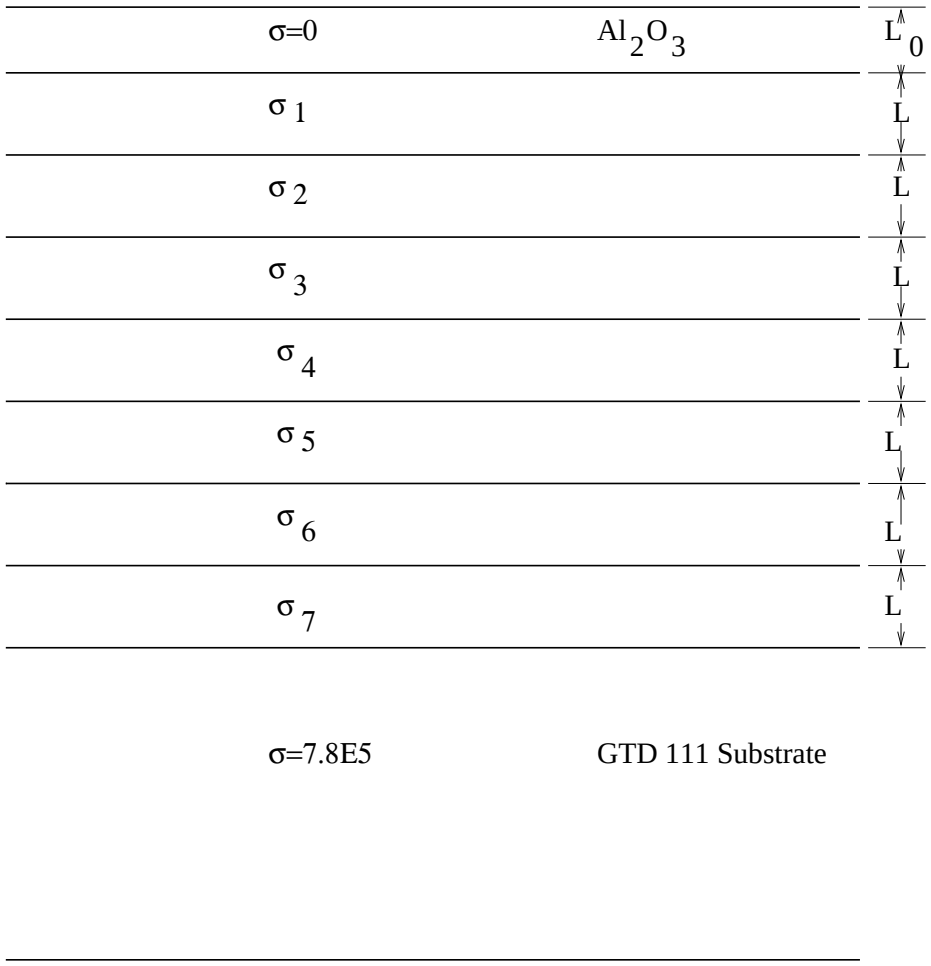

Figure 13: The 8-layer inversion algorithm, in which L is the given resolution, and the objective is to determine L_0 and σ_1 through σ_7.

done by a process of nonlinear least-squares, in which the eight variables are chosen to give the best fit to the impedance data. The inversion is done in several steps, starting with the computation of a table of data, from which the final solution is determined by interpolation. The process is quite fast, and is quite conservative in computational resources.

Example 1: 12-layer Model of a GT33+ Coating. We will apply the 12-layer algorithm to

the model of the GT33+ substrate that is shown in Figure 1. L_0, the length of the Al_2O_3 layer is 30 microns, and the lengths of the $\beta+$ and β layers are each 100 microns. The inter-diffusion zone, IZ, is given as 20 microns. Each of the eleven layers within the coating + workpiece is given as 24 microns, which means that the problem depth extends to 264 microns. The liftoff of the coil is presumed to be 1 mil (= 25.4 microns), which is the actual depth of the coil within the acrylic box that was used in the PWA286 and GT33+ experiments.

The numerical experiment is run at the 33 frequencies (in MHz): 0.684, 0.81, 0.947, 1.094, 1.252, 1.421, 1.6, 1.79, 1.991, 2.202, 2.424, 2.656, 2.899, 3.153, 3.418, 3.693, 3.979, 4.275, 4.582, 4.9, 5.228, 5.567, 5.917, 6.278, 6.649, 7.03, 7.422, 7.825, 8.239, 8.663, 9.098, 9.544, 9.999. These are the frequencies that CESI used in the demonstration of their system at EPRI-Charlotte in May 2002. We do not know why this sequence of frequencies was chosen, but it is what we used in the exercise.

The **VIC-3D©** run produced the following results:

Variable No.	1	2	3	4	5	6	7	8	9	10	11	12
$\sigma(\times 10^5)$	9.85	12.3	12.8	11.7	10.3	9.03	8.05	7.33	6.82	6.47	6.24	54.4μ
Sensit$(\times 10^{-4})$	4.74	5.92	7.57	9.85	12.7	16.3	20.6	25.8	32.2	39.9	49.3	1.30

The first eleven variables are the conductivities of the eleven layers (from top to bottom), and the twelfth variable is the thickness of the aluminum-oxide layer, measured in microns, plus the liftoff of the coil. When we subtract the liftoff, we are left with a value of 29 microns for the thickness of the oxide coating. The third row lists the 'sensitivity coefficients' of the solution. This will be defined in the discussion of nonlinear parameter estimation that is given in the next section. Suffice it to say that the smaller the number the more sensitive the solution to that particular variable. Hence, we see that the solution is most sensitive to the thickness of the oxide coating, with decreasing sensitivities to the deeper layers, as we would expect in a one-dimensional layer problem of this type with excitation and detection occuring only above the workpiece

In order to determine the conductivities of the $\beta+$ and β layers, we average the results over 2 100-micron slabs, the first being the $\beta+$ layer, and the second the β layer. Remembering that each (mathematical) layer of the inversion algorithm is 24 microns, we have

$$\begin{aligned} 24 \times (9.85 + 12.3 + 12.8 + 11.7) + 4 \times 10.3 &= 1160.6 \\ &= 100 \times \beta + \\ 20 \times 10.3 + 24 \times (9.03 + 8.05 + 7.33) + 8 \times 6.82 &= 846.4 \\ &= 100 \times \beta \end{aligned} \tag{1}$$

From this we conclude that the conductivity of the $\beta+$ layer is 11.61×10^5 S/m and of the β layer 8.46×10^5 S/m.

Finally, in order to calculate the thickness of the inter-diffusion zone, we average over the last 64 microns of the problem grid, which we know must contain both the IZ and GTD111. The average conductivity of these 64 microns is $(16 \times 6.82 + 24 \times (6.47 + 6.24))/64 = 6.47(\times 10^5$, of course). Keeping in mind that the conductivity of the IZ is 3.32×10^5 S/m and of the GTD111 substrate 7.8×10^5 S/m, we get that the percentage, L, of the 64 microns that is covered by the IZ is given by $6.47 = 3.32 \times L + 7.8 \times (1. - L)$, or $L = 0.297$. From this we get that the length of IZ is $0.297 \times 64 = 18.98$. We summarize these results in the following table:

	Computed	Original
$\beta+$	11.61×10^5	12.0×10^5
β	8.46×10^5	8.4×10^5
IZ	18.98 microns	20.0 microns
Al_2O_3	29.0 microns	30 microns

Example 2. 8-layer Inversion of Laboratory Data for the PWA286 Coating. The PWA286 coating is more complicated metallurgically than the GT33+, because, as the aluminum diffuses out to reform the protective oxide coating, and also diffuses into the substrate, there occurs a transformation of beta phase NiAl into a gamma matrix of solid nickel solution, which does not appear in the GT33+ coating. This gamma matrix manifests itself as a beta-phase depleted zone (called 'Zone1'), resulting in a 'standard model' shown in Figure 14. Further, while the conductivity of the various zones remains fixed over time, the layer-thicknesses of these zones changes. This presents a problem that is dual to the GT33+, in which the conductivity changes, while the thickness of the β+ and β zones remains fixed. The PWA286 problem is a more inverse problem.

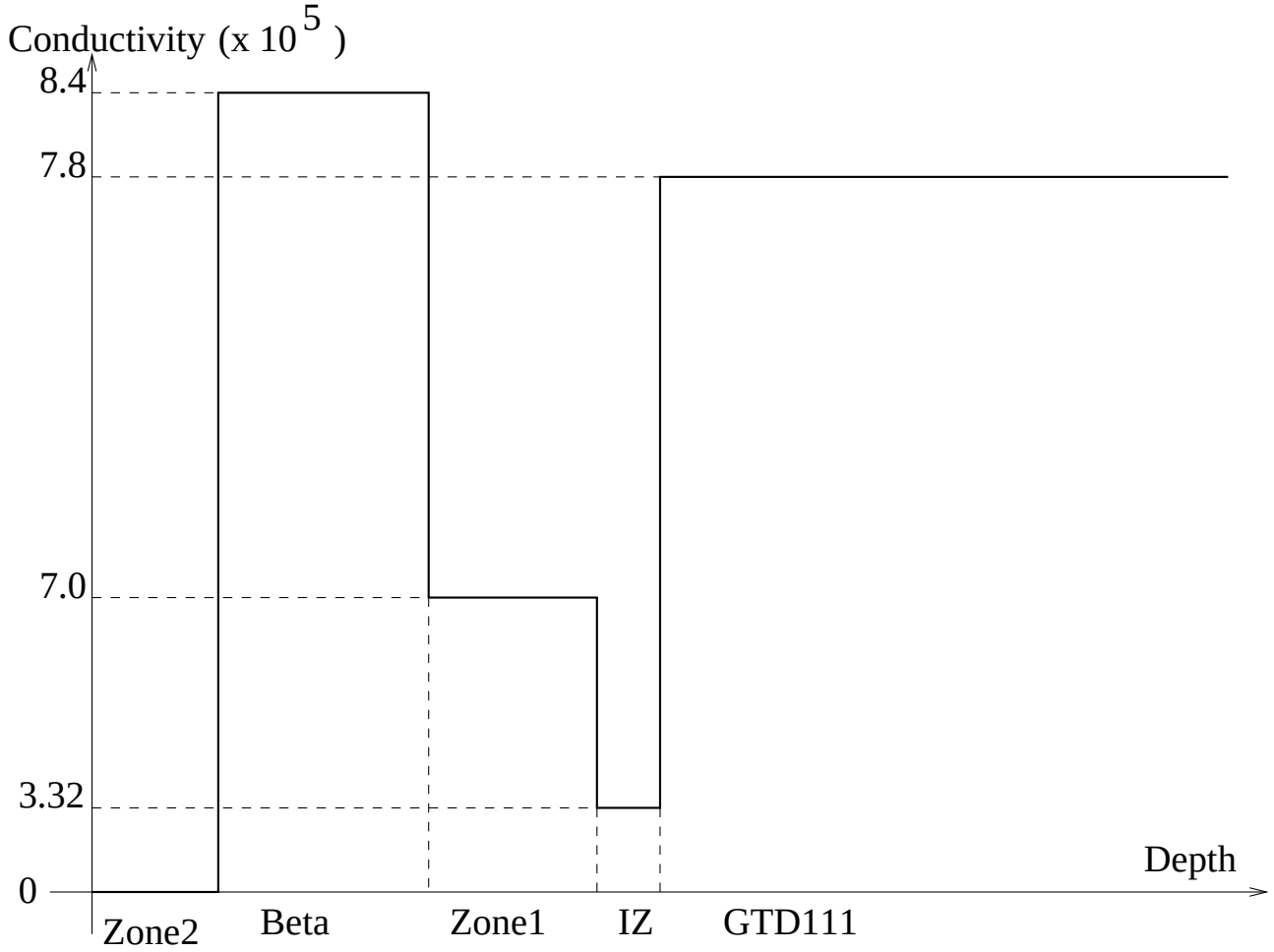

Figure 14: Standard model of the PWA286 thermal barrier coating. The conductivities are determined from measurements on known samples.

Using the same setup as for the GT33+, we took laboratory data on a number of coupon-samples of PWA286 coatings that had undergone various levels of deterioration. The measured impedances are shown in Figure 15. It should be noted, once again, that these data are cleaner than the corresponding data for the GT33+, which should not be too surprising, since the measurements were taken at least two-years apart. We then applied the 8-layer algorithm, in very much the same manner as described above, to invert these data.

The results of the inversion process are fitted to the 'standard model' of the PWA286 TBC,

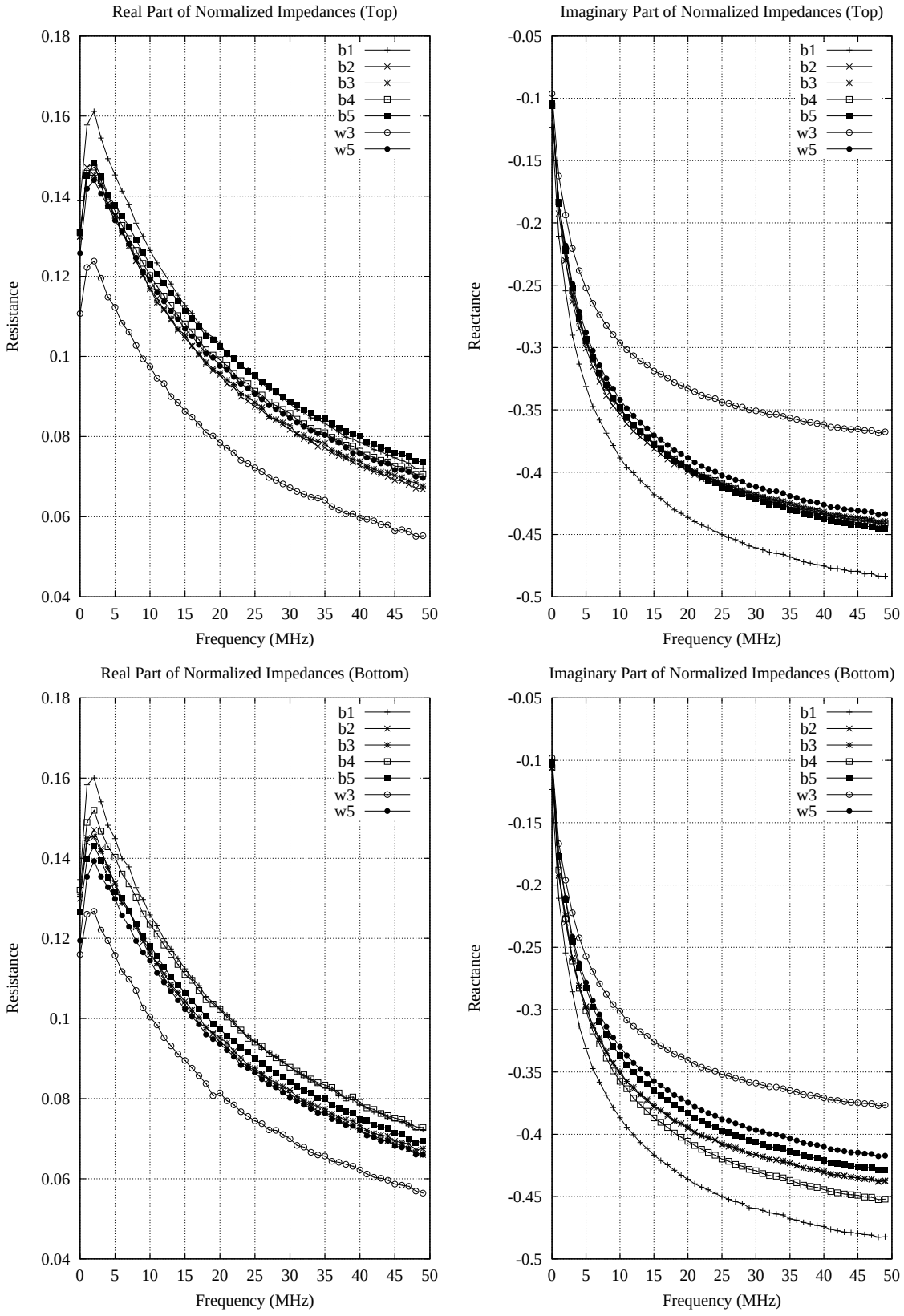

Figure 15: Real (left) and imaginary (right) parts of the normalized change in impedance for the 'top' PWA286 samples (upper two figures) and 'bottom' PWA286 samples (lower two figures).

that is shown in Figure 14. The values of the conductivity of the various layers are determined from inversions on known samples. In this manner, we are able to determine the thickness of each zone. The results are tabulated in Tables 2 and 3.

Sample Identification	Coating Location	Coating Identification	Average Thickness (microns)	Computed Thickness (microns)
1950F-"as coated" (Blue-1)	Top Side	Inner Diffusion	10.6	10.0
		Inner Beta Depleted	–	–
		Beta Phase Zone	132.0	132.0
		Outer Beta Depleted	–	–
	Bottom Side	Inner Diffusion	10.1	10.0
		Inner Beta Depleted	–	–
		Beta Phase Zone	140.9	142.0
		Outer Beta Depleted	–	–
1950F-250 cycles (Blue-2)	Top Side	Inner Diffusion	22.4	20.0
		Inner Beta Depleted	8.9	9.4
		Beta Phase Zone	122.4	120.0
		Outer Beta Depleted	14.5	17.7
	Bottom Side	Inner Diffusion	22.2	22.6
		Inner Beta Depleted	8.1	9.1
		Beta Phase Zone	114.2	112.5
		Outer Beta Depleted	11.6	20.0
1950F-500 cycles (Blue-3)	Top Side	Inner Diffusion	24.4	26.3
		Inner Beta Depleted	14.9	14.4
		Beta Phase Zone	94.6	93.0
		Outer Beta Depleted	17.9	19.2
	Bottom Side	Inner Diffusion	24.8	28.2
		Inner Beta Depleted	16.8	15.3
		Beta Phase Zone	98.0	94.5
		Outer Beta Depleted	19.7	19.7

Table 2: Comparison of measured and computed coating thicknesses for the PWA286 test.

In several cases, the final computed conductivity profiles were obtained by a process of 'focussing' the 8-layer inversion algorithm. This is accomplished by starting with a rather coarse grid, which allows the Beta Aluminide Zone and Interdiffusion and Inner Beta Depleted Zone 1 to be generally located relative to the GTD111 Substrate. Then we refine the grid between the Beta Aluminide Zone and GTD111 Substrate to get a more precise value for the various zone boundaries, as well as a more precise value for the conductivity of Zone 1 and the Interdiffusion Zone. In this manner, we were able to locate the Interdiffusion Zone, and determine its conductivity for the 'as-coated' samples, B1B and B1T. This is a fairly difficult computation to carry out without such a 'multigrid rezoning' technique.

The tabulated results confirm that the inversion algorithm produces excellent reconstructions, with very good resolutions. In particular, we note the good agreement between the computed and measured thickness of the beta-zone of each sample. This is the critical datum, when it comes to determining the remaining life of the thermal barrier coating.

Sample Identification	Coating Location	Coating Identification	Average Thickness (microns)	Computed Thickness (microns)
1950F-1000 cycles (Blue-4)	Top Side	Inner Diffusion	25.8	26.4
		Inner Beta Depleted	34.0	33.0
		Beta Phase Zone	62.6	63.8
		Outer Beta Depleted	37.5	41.5
	Bottom Side	Inner Diffusion	23.7	25.0
		Inner Beta Depleted	38.1	40.1
		Beta Phase Zone	52.6	53.0
		Outer Beta Depleted	33.2	34.8
1950F-1938 cycles (Blue-5)	Top Side	Inner Diffusion	23.6	24.0
		Inner Beta Depleted	118.7	119.0
		Beta Phase Zone	–	–
		Outer Beta Depleted	–	34.3
	Bottom Side	Inner Diffusion	28.4	25.0
		Inner Beta Depleted	61.5	64.0
		Beta Phase Zone	15.2	16.0
		Outer Beta Depleted	48.5	46.3
1850F-3500 cycles (White-5)	Top Side	Inner Diffusion	13.5	13.7
		Inner Beta Depleted	46.0	45.2
		Beta Phase Zone	35.2	34.8
		Outer Beta Depleted	50.2	44.6
	Bottom Side	Inner Diffusion	14.2	15.1
		Inner Beta Depleted	45.9	45.5
		Beta Phase Zone	27.6	29.6
		Outer Beta Depleted	46.9	53.1

Table 3: Comparison of measured and computed coating thicknesses for the PWA286 test.

CONCLUSIONS ABOUT THE GT33+ DUPLEX COATING

Our first conclusion is that the GTD111 substrate has a conductivity of 7.8×10^5 S/m, as in the PWA286 model. This was verified at the outset, in order to remove a variable from the Sample A, Sample B, and Sample E problems. By using impedance measurements (real and imaginary components) over the frequency range of 1-50 MHz, we gain insight into the status of each coating. High-frequency measurements of the normalized reactance give us a good estimate of the thickness of Z2, which, in turn, gives us some insight into the status of the coating, because this layer consists of Al_2O_3, which grows by the 'sacrifice' of the $\beta+$ overlay coating and/or the β bond coat. Furthermore these high-frequency measurements, especially of the normalized resistance, help us to estimate the conductivity of $\beta+$, which is a principal determinant of the remaining life of the coating. Lower frequencies are useful in determining the conductivity of the β layer.

Next, we conclude that the Z2 layer of Sample A has a thickness of about 55 microns, with the $\beta+$ layer having a conductivity of between 7×10^5 and 8×10^5 S/m, and the β layer having a conductivity of 6×10^5 S/m. This corresponds to a $\beta-$depleted layer.

Sample E is the best of the three, having a Z2-thickness of 30 microns, a $\beta+$ conductivity of close to 1.2×10^6 S/m, and a $\beta-$conductivity of 8.4×10^5 S/m. Indeed, if we assume that an 'as-coated' sample has a $\beta+$ conductivity of 1.2×10^6 S/m, and a β conductivity of 8.4×10^5 S/m, as in the PWA286 coating, then Sample E is almost in an as-coated condition.

Sample B is the most confusing to interpret. The results indicate a Z2 depth of only 15 microns, whereas the $\beta+$ and β layers have a conductivity of only about 5×10^5 S/m. These low conductivities suggest that the layer is well-worn, which should correspond to a much larger value of the thickness of Z2. Perhaps much of Z2 has been ablated during use, and we see only a small residual, but the more likely explanation is that we are sensing the presence of 'crazed cracking' in the coating, which would invalidate the simple one-dimensional four-layer model that we are using.

These results agree with the metallurgical examinations as conveyed to us in an email of 14OCT02.

References

[1] Electric Power Research Institute, 'Performance Demonstration Protocol For Round Robin Testing of Combustion Turbine Blade Coatings,' privately distributed, Summer 2000.

[2] Ogawa, K., T. Shoji, I. Abe, and H. Hashimoto, '*In situ* NDT of Degradation of Thermal Barrier Coatings Using Impedance Spectroscopy,' Materials Evaluation/March 2000, pp. 476-481.

[3] Strangman, T. E., 'Thermal Barrier Coatings for Turbine Airfoils,' *Thin Solid Films*, Volume 127, 1985, pp. 93-105.

[4] Harrison, D.J., L. D. Jones, and S. K. Burke, 'Benchmark Problems for Defect Size and Shape Determination in Eddy-Current Nondestructive Evaluation,' Journal of Nondestructive Evaluation, Vol. 15, No. 1, 1996, pp. 21-34.

[5] A. H. G. Rinnooy Kan, G. T. Timmer, "Stochastic Global Optimization Methods Part I: Clustering Methods," Mathematical Programming 39 (1987), pp. 27-56.

[6] A. H. G. Rinnooy Kan, G. T. Timmer, "Stochastic Global Optimization Methods Part II: Multi Level Methods," Mathematical Programming 39 (1987), pp. 57-78.

[7] R. H. Byrd, C. L. Dert, A. H. G. Rinnooy Kan, R. B. Schnabel, "Concurrent Stochastic Methods for Global Optimization," Mathematical Programming 46 (1990), pp. 1-29.

[8] J. M. Wozencraft and I. M. Jacobs, *Principles of Communication Engineering*, John Wiley and Sons, New York, 1965.